CrossMark

ORIGINAL PAPER

Effects of different metals on the synthesis and properties of waterborne polyurethane composites containing pyridyl units

Chi-Hui Tsou[1] · Hsun-Tsing Lee[2] · Wei-Song Hung[3] ·
Manuel De Guzman[3] · Szu-Ting Chen[4] · Maw-Cherng Suen[4] ·
Sigi Tri Wicaksono[5]

Abstract This study used dicyclohexylmethane 4,4-diisocyanate, polybutylene adipate, polyether-1,3-diol, and 2,6-pyridinedimethanol to synthesize a novel water-based polyurethane (WPU) that contained pyridyl units. To enhance the thermal, mechanical, swelling, and antimicrobial properties of the WPU, various metals (silver nitrate, copper acetate, cobalt acetate, and zinc acetate) were incorporated to form WPU/metal composites. In addition, the study investigated the effects of the metal types on the WPU properties. Fourier transform infrared spectroscopy was used to confirm the synthesis of the WPU containing pyridine. Atomic force microscopy illustrated that the added metals increased the WPU surface roughness. The contact angle and degree of swelling tests demonstrated that the added metal reduced the WPU hydrophilicity, and with the addition of other metal types, the hydrophobicity increased considerably. Thermal gravimetric analysis indicated that the initial decomposition temperature of the highest WPU thermal stability was attributed to zinc. In addition, the results of differential scanning calorimetry and dynamic mechanical analysis showed that adding a small amount of metal increased the hard and soft segment glass transition temperatures. A universal strength tester validated that the WPU mechanical properties varied with the different metal

✉ Maw-Cherng Suen
  sun@tiit.edu.tw

[1] Department of Materials Science, Chulalongkorn University, Bangkok 10330, Thailand

[2] Department of Chemical and Materials Engineering, Vanung University, Jongli, Taoyuan 32091, Taiwan, ROC

[3] R&D Center for Membrane Technology, Chung Yuan University, Jongli, Taoyuan 32023, Taiwan, ROC

[4] Department of Creative Fashion Design, Taoyuan Innovation Institute of Technology, Jongli, Taoyuan 32091, Taiwan, ROC

[5] Department of Materials and Metallurgical Engineering, Institut Teknologi Sepuluh Nopember, Sukolilo, Surabaya 60111, Indonesia

🙋 Springer

additives and that the WPU strength increased. However, the WPU toughness and ductility decreased with the addition of metals; silver provided the highest mechanical strength. An antimicrobial test indicated that silver enhanced the antimicrobial property. The moisture permeability and waterproof property of the WPU coating was also analyzed.

Introduction

Waterborne polyurethanes (WPUs) are versatile, environment-friendly materials used in coatings and adhesives for wood, in automobiles and in numerous flexible substrates, such as rubber, leather, paper, and textiles [1–6]. Several features of WPUs relate to those of the traditional solvent-borne PUs (low viscosities at high molecular weights).

New environment-friendly PU materials were obtained by the glycolysis of waste PU [7] or natural oil [8, 9]. Datta [9] synthesized biopolyurethanes from hydroxylated soybean oil and biobased propanediol. Tsou et al. [10] synthesized a new type of PU by curing a prepolymer with moisture. The new polymers prepared by several studies [7–11] show good performance and high tensile properties. Mohamed et al. [12] reported a novel study about castor oil-based WPU, containing PU-aromatic polyamide sulfone copolymer, which was prepared using ethylene diamine as a chain extender for a prepolymer-ionomer synthesized from castor oil. However, the insolubility, thermal stability, and mechanical properties of WPUs were lower than those of organic-solvent-borne PUs [13]. Using fillers is an effective method to enhance the properties of WPUs. Various types of additives—such as multiwalled carbon nanotubes [14–17], Ag [17, 19], Au [20], Cu [21], ZnO [22], cellulose [23, 24], and clay [25–27] —have been studied, and the results demonstrated that the additives' mechanical properties and thermal stabilities substantially enhanced the performance of composite materials. Mu et al. [17] researched on modifying multiwalled carbon nanotubes through a novel biomimetic approach; they were used for enhancing the mechanical properties of PU. Hsu [18] reported that WPUs containing silver nanoparticles were biocompatible and exhibited antibacterial properties. Zhao [21] indicated that copper improved the antibacterial activity and thermal stability. Datta et al. [28] synthesized PU elastomers from oligo(oxytetramethylene)diol, which showed high mechanical properties. However, there are only a few reports about the comparison of different metals in WPUs. Furthermore, the application of WPUs on breathable waterproof fabric coatings requires water resistance, and the balance of water vapor permeability requires additional studies. The prepolymer was prepared from dimethylol butanoic acid, isophorone diisocyanate, and a copolymer of ethylene oxide and propylene oxide [29].

In our recent study [30], we synthesized a new pyridine-containing chain extender—bis(3-pyridinemethanol) silver—which was used to produce an antimicrobial PU. In another study [31], we used aromatic 2,6-pyridinedimethanol (2,6-PDM) as a chain extender for polycaprolactone and dicyclohexylmethane 4,4-diisocyanate (MDI) to create a novel PU. Compared with a standard aliphatic chain

extender, 2,6-PDM should be capable of improving the tensile strength of the resultant PU to a higher degree. However, pyridine moieties in WPUs have never been studied. On the basis of the promising results of using 2,6-PDM and metals with enhanced thermal, mechanical, and antibacterial properties, our present study used $H_{12}MDI$, polybutylene adipate (PBA2000), polyether-1,3-diol (D-3403), and 2,6-PDM to synthesize a novel WPU that contained pyridyl units. The effects of various metals on the mechanical, thermal, swelling, and antibacterial properties of WPU/metal composites were determined using Fourier transform infrared spectroscopy (FTIR), thermogravimetric analysis (TGA), differential scanning calorimetry (DSC), dynamic mechanical analysis (DMA), scanning electron microscopy, and tensile tests. Finally, WPU and WPU/metal composites were used as a coating agent to improve the waterproofness of fabrics.

Experimental

Preparation of waterborne polyurethane and its metal composites

First, PBA2000, D-3403, and 2,2-dimethylolpropionic acid (DMPA) were poured into a 4-opening reaction tank equipped with devices such as a set-speed mixer and a thermostat. Next, the solution was heated at 100 °C for 20 min to remove the water. The following materials were purchased from Aldrich: MDI ($M = 262$ g/mol); 2,6-PDM ($M = 139.15$ g/mol); and multiple drops of the catalyst dibutyltin–dilaurate 95 % (T-12, $M = 631.25$ g/mol). The catalyst was diluted to 5 % using N,N-dimethylacetamide ($M = 87.12$ g/mol, Mallinckrodt Chemicals) and was introduced into a reactor at 80 °C, operating at 300 rpm. The solution was left in the reactor for 2.5 h to obtain a prepolymer containing NCO at the endpoint. The prepolymer was titrated to determine the free NCO content (close to the theoretical value). The acetone processing method was used to separate the materials, forming WPU dispersions. After the temperature dropped to 55 °C, triethylamine (TEA, $M = 101.19$, Nihon Shiyaku Industries) was added to neutralize the product for 20 min. Next, the rpm was increased to 1000, and the polymer was mixed with 65 wt% deionized water before it was dispersed evenly in water. The final step was a 30-min reaction involving a chain-extended ethylene-diamine (EDA, $M = 60.1$ g/mol, Aldrich); a pyridine-filled WPU (35 %) was obtained. Scheme 1 shows the steps in synthesizing the WPU emulsion. The metal solution (metal/50 g of water) was added to a pure WPU that was prepared at 1000 rpm, and the solution was reacted for 30 min, resulting in a pyridine-filled WPU/metal emulsion. The WPU/metal emulsions were placed in a dish at room temperature for 2 days, and then the films were moved to a Teflon membrane plate in the oven at 50 °C for 24 h. The last step was heat treatment at 100 °C for 2 min, then the films were kept in a dry cabinet. The thickness of each film was about 0.03 mm ± 0.005 mm. Scheme 2 shows the chemical reaction involved in synthesizing WPU/metals composites. The dipolar bond of pyridine with metal was reported in our previous study [30]. The calculation of the metal quantity is as follows: 2,6-PDM (equivalent) × the metal added (10 %) × the metal's molecular
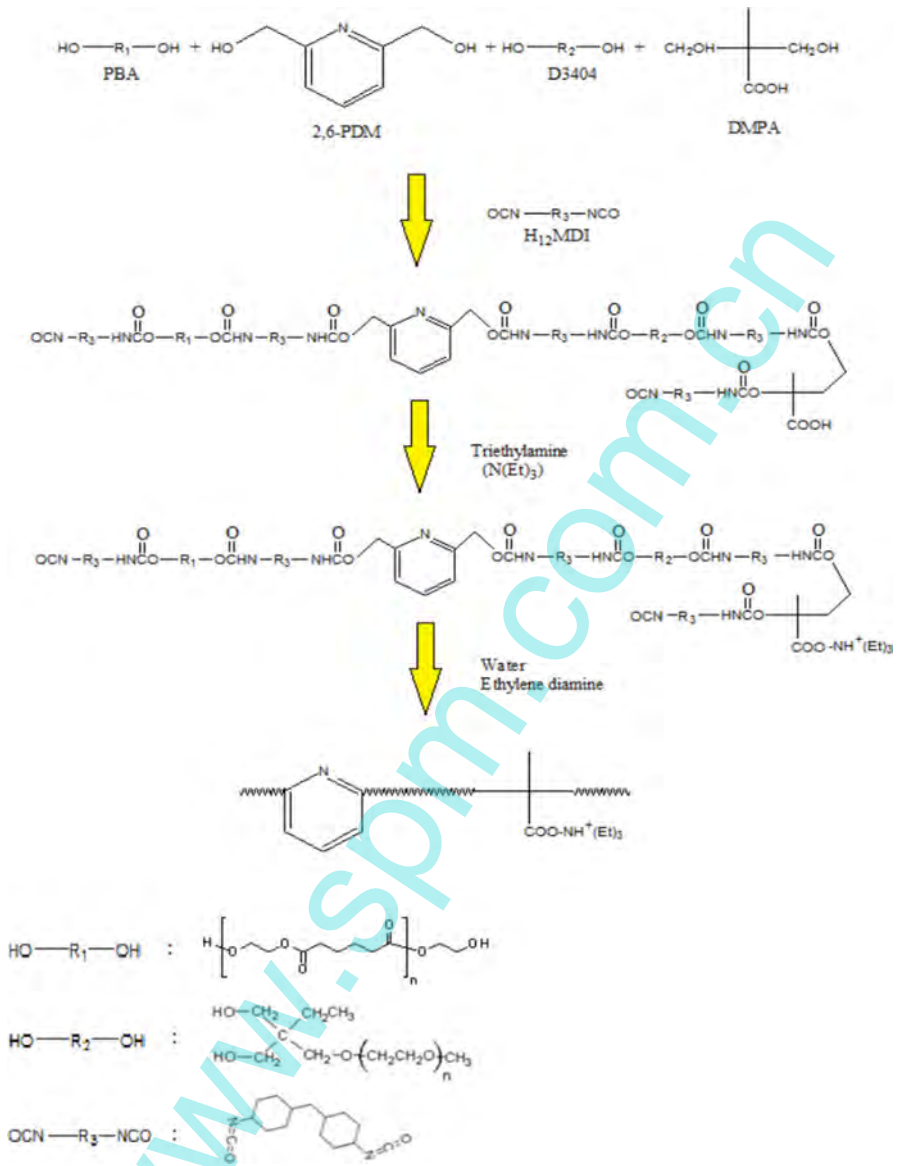
Scheme 1 Synthesis of WPU

weight = the required quantity of the metal to be added (g). For example, if the metal is Ag: $0.018 \times 10\ \% \times 169.87 = 0.306$ g. The data for WPU and WPU/metal composites are given in Table 1.
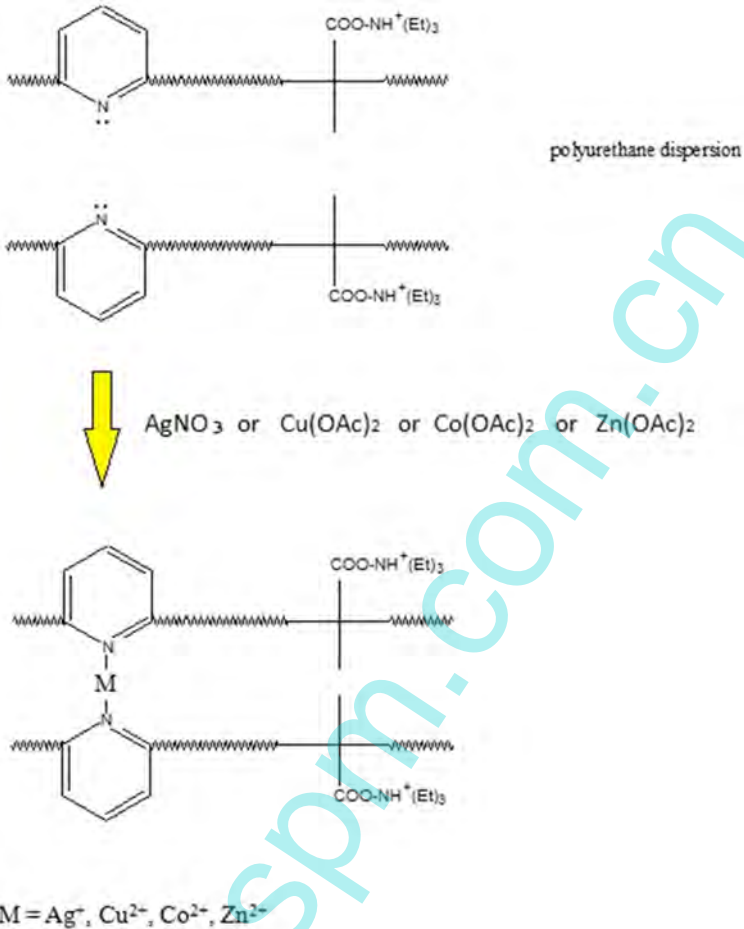
Scheme 2 Synthesis of WPU/metal composites through a dipolar bond reaction

Fourier transform infrared

FTIR measurements were conducted using a PerkinElmer spectrometer (model Spectrum One). The spectra of the samples were obtained by averaging 15 scans with a wavenumber range of 650–4000 cm^{-1} and a resolution of 2 cm^{-1}.

Laser diffraction particle size and viscometry

The average metal particle size distribution in the emulsion was measured by a laser scattering size distribution analyzer (HORIBA, model LB-550). The average viscosity of the WPU/metal composites was measured by BROOKFIELD (model DV-E VISCOMETER).

Table 1 WPU and WPU/metal composites

Sample	Metal types	Equivalent							
		0.0018 Metals (g)	0.033 PBA (g)	0.018 D-3403 (g)	0.018 22,6-PDM (g)	0.0552 DMPA (g)	0.1987 H_{12}MDI (g)	0.0497 TEA (g)	0.0745 EDA (g)
WPU									
W-Ag	$AgNO_3$	0.306							
W-Cu	$Cu(OAc)_2$	0.359	33	10.98	1.251	3.698	26.03	2.51	2.235
W-Co	$Co(OAc)_2$	0.448							
W-Zn	$Zn(OAc)_2$	0.395							

Atomic force microscopy

Atomic force microscopy (AFM) was used to analyze the surface morphology of the polymer samples. AFM analysis was performed in air using a Being Nano-Instrument (model CSPM5500). During the analysis, the microscope was operated in a tapping mode with a scanning rate of 0.5 Hz for all scanning sizes using an etched silicon probe ($k = 50$ N m^{-1}). From the AFM images on a 5.0×5.0 μm^2 area, the root mean square roughness (Ra) of the topographic profiles was evaluated. For each sample, several images on different spots were acquired, and after that, the average roughness was calculated.

Contact angle

Contact angles (CAs) were measured with deionized water using a FACE (model CA-VP150) instrument at room temperature. Each sample was prepared by cutting it into test pieces of 30×30 mm^2. The CAs were recorded as the water was added onto the surface of each sample or withdrawn from the drop on the sample surface with a syringe pump. The CA reported was an average value for 3–4 drops. For a liquid drop resting on a flat, horizontal solid surface, the CA is defined as the angle formed by the intersection of the liquid–solid interface and the liquid–vapor interface (geometrically acquired by applying a tangent line from the contact point along the liquid–vapor interface in the droplet profile).

Swelling degree

A film specimen with a dimension of 3×3 cm^2 was dried to a constant weight in a circulating oven at 120 °C. Subsequently, the dried specimen was placed in a sealed conical flask containing 100 mL of 20 wt% aqueous ethanol solution. It was kept there for 24 h. The swollen specimen was then removed from the flask, wiped with a filter paper, and weighed. The swelling degree was calculated according to the following equation:

$$\text{Swelling degree} = \frac{W_{w} - W_{d}}{W_{d}} \times 100\%,$$

where W_{d} = weight of the dried film and W_{w} = weight of the swollen film.

Energy dispersive X-ray spectroscopy

The specimen (1–2 mm^2) morphology was observed using energy dispersive X-ray spectroscopy (EDS, 7021-H HORIBA). It was sputtered first with gold dust before placing it in the instrument. Then, the measurement was initiated. The spectroscope was operated at 15 kV.

Thermogravimetric analysis

Thermogravimetric analysis (TGA) was obtained using a PerkinElmer TGA (model Pyris 1). The samples (8–10 mg) were heated from room temperature to 700 °C under nitrogen at a rate of 10 °C/min.

Differential scanning calorimetry

Differential scanning calorimetry (DSC) tests were run on a PerkinElmer DSC (model Jade). The samples were sealed in aluminum pans. Scans (−100 to 80 °C) were conducted with a heating rate of 10 °C/min under nitrogen purging. Glass transition temperatures (T_g) were recorded on the basis of the maximum peak of the endothermic transition in the second scan. Samples of approximately 7–8 mg were used for all the tests.

Dynamic mechanical analysis

Dynamic mechanical analysis (DMA) was performed using TA DMA (model Q800) at 1 Hz with a 5-μm amplitude over a temperature range of −80 to 100 °C and at a heating rate of 3 °C/min. DMA was conducted with a tension mode and a specimen dimension of 20 × 5 × 0.2 mm ($L \times W \times H$). The T_g was equivalent to the peak temperature of the glass transition region in the tan δ curve.

Stress–strain test

The tensile strength and elongation at break were measured using a universal testing machine (model QTest 5). The testing was conducted according to ASTM D638. The film specimens had dimensions of 45 × 8 × 0.2 mm.

Antibacterial evaluation

The antibacterial activity of the WPU/metal composites was tested against aerobic bacteria commonly found on burn wounds: *S. aureus* (ATCC 25023) and *K. pneumoniae* (ATCC 13883). The assessment was conducted on the basis of the disc diffusion method of the US Clinical and Laboratory Standards Institute. Both the neat WPU and AgNO$_3$-containing PU were cut into circular discs (15 mm in diameter). Vancomycin was used as the control antibacterial drug. The specimens were used for *S. aureus* and *K. pneumoniae*. Each specimen and each control drug were placed on a Difco^{TM} Mueller Hinton agar in a Petri dish, which was then

incubated at 37 °C for 24 h. If inhibitory concentrations were reached, there would be no growth of microbes, seen as a clear zone around the disc specimens. The specimens were photographed for further evaluation.

Fabricating waterborne polyurethane films and fabric coating

To fabricate WPU films, the correct amount of emulsion was placed in a Petri dish and dried at room temperature for 2 days. The film was then placed on a Teflon board and kept in an oven and heated at 50 °C for 1 day. Next, the film was heated at 100 °C for 2 min before it was moved and preserved in a moisture proof container. Thereafter, various physical and chemical tests on the specimen were conducted. For the fabric coating process [29], a thickener was added to the WPU. After mixing the materials evenly, they were coated on a nylon fabric using a coating rod and placed inside the oven, and heating was initiated at 60 °C for 5 min. Then, the temperature was increased every minute by 4 °C until it reached 100 °C.

Water vapor permeability and waterproofness analyses of fabrics coated with a waterborne polyurethane

A WPU containing a metal of a certain amount was coated on a nylon fabric to test its waterproofness and water vapor permeability (WVP). The WVP refers to the time required for a set amount of water vapor to pass through a surface area at a predetermined temperature and humidity. It is typically described as $g/m^2 \times 24$ h. In general, PU-coated fabrics acquire WVP and waterproofness using microporous or nonporous hydrophilic PU films. By applying microporous films, water drops are unable to penetrate the fabric coating, whereas water vapors are able to penetrate. Using nonporous hydrophilic films, water vapors can penetrate the hydrophilic areas of coated fabrics through absorption, proliferation, and desorption.

Results and discussion

Fourier transform infrared

Figure 1 shows the FTIR absorption spectra of different WPU films with and without a metal additive. An absorption band between 3600 and 3200 cm^{-1} signified the presence of a functional group containing hydrogen bonding including O–H bonds from alcohols or acids and N–H bonds from amines or their salts. Between 3500 and 3200 cm^{-1}, there was an absorption band in the O–H bonds of alcohols and a wide and strong absorbing band in the O–H bonds of the carboxylic acid. The N–H bonds of amines or their salts had absorption peaks with dissimilar characteristics between 3500 and 3300 cm^{-1}.

Wide absorption bands between 3600 and 3200 cm^{-1} are attributed to N–H functional groups, such as amine salts and urethane, which are found in the WPU structure. Within such an interval, carboxylic acid functional groups were not observed, indicating that carboxylic acids from DMPA were entirely neutralized by
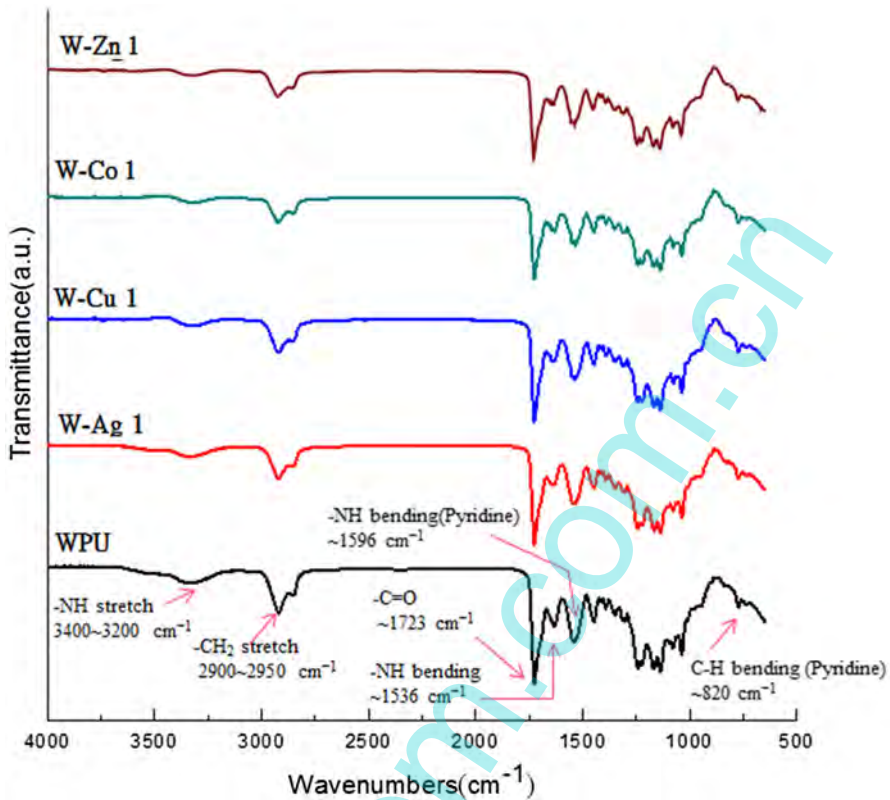
Fig. 1 FTIR of WPU and WPU/metal composites

TEA. The absorption range for C–H bonds was 3600–3200 cm^{-1}. The stretching vibration absorption peak of alkyl (–CH$_2$) bonds was between 2949 and 2950 cm^{-1}. An absorption peak for isocyanate (–N=C=O) was not observed between 2250 and 2285 cm^{-1}, and an absorption peak at 1723 cm^{-1} refers to the characteristic peak of carboxyl, which was formed by urethane functional groups. Scheme 1 describes the equation of the reaction.

Because carboxylate possesses a resonance phenomenon, two absorption peaks were observed between 1629 and 1442 cm^{-1}. Benzene ring (N–H bond) bending–stretching vibration was observed at 1596 cm^{-1}. The absorption peak at 1536 cm^{-1} refers to the absorption of urethane secondary amine N–H bonds. The absorption peak between 1350 and 1000 cm^{-1} included C–N and C–O bonds. The absorption peak at 1233 cm^{-1} refers to the absorption of urethane carbon–oxygen (C–O) bonds. The bending–vibrating absorption peak of C–H in the pyridine rings at 820 cm^{-1} verified the synthesis of WPUs [1, 13, 16].

Particle size and viscosity analysis

Table 1 shows various WPUs, depending on the metal additive. The second and third columns in Table 2 list the particle size and viscosity (at room temperature and 100-rpm rotor rate) of the metal composites, respectively. The results indicate that different metals caused various particle sizes of the WPUs. Their sizes in descending order were W-Ag > W-Zn > W-Cu > W-Co. This phenomenon is attributed to the different atomic radii of the metals; the radii of Ag, Zn, Cu, and Co atoms are 1.34, 1.25, 1.17, and 1.16 Å, respectively. Figure 2 shows the particle size distribution of WPUs with and without a metal additive.

The viscosity analysis in Table 2 shows that the WPU viscosity increased with the addition of a metal, which indicates that a metal additive can change the surface shear stress, resulting in disrupting the rheological activities and increasing the viscosity. The largest viscosity change was observed with the addition of Cu, where the viscosity increased from 9.5 to 11.6 cps.

Surface roughness analysis

AFM is chiefly used to determine and analyze the effect of different metals on the material surface roughness. Figure 3 shows a 3D image of the surface of pyridine-filled WPU/metal composites. The Ra for each sample indicated that the WPU roughness increased as a result of adding a metal (Table 2); for W-Ag, the Ra increased from 0.88 to 2.02 nm. In descending order, the Ra of the WPUs was W-Ag > W-Cu > W-Co > W-Zn. This result indicates the differing effects of various metals on the surface roughness; the greatest roughness was observed for Ag, whereas the least was observed for Zn.

Contact angle analysis

Figure 4 presents the contact angle measured for each sample. The contact angle data in Table 2 denote the effect of a metal additive on the WPU hydrophilicity—the contact angle increased on the addition of a metal, indicating that the presence of a metal caused the material to become hydrophobic.

A previous study [34] reported that under normal circumstances, the rougher a surface was, the greater the liquid contact angle became [34]. On the basis of the

Table 2 Particle size, viscosity, average roughness, contact angle, and degree of swelling of WPU and WPU/metal composites

Sample	Particle size (nm)	Viscosity (cps)	Ra (nm)	Contact angle (°)	Degree of swelling (%)
WPU	113	9.5	0.88	52.0	31.2
W-Ag	219	11.3	2.02	63.1	30.1
W-Cu	172	11.6	1.99	62.1	30.2
W-Co	150	11.2	1.58	59.7	30.3
W-Zn	190	11.3	1.26	55.4	30.4
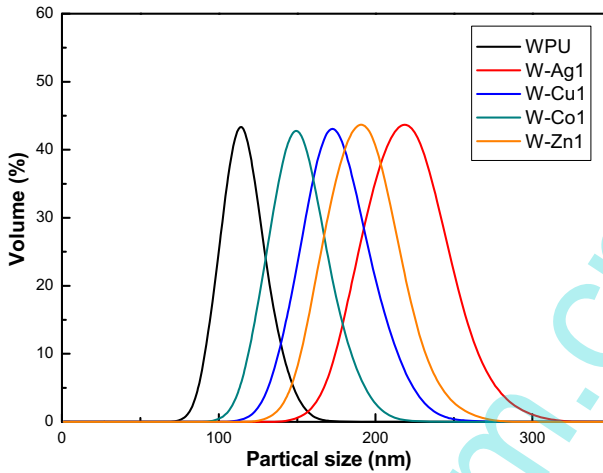
Fig. 2 Particle size distributions of WPU and WPU/metal composites

AFM analysis discussed in the previous section, the WPU roughness increased on the addition of a metal. Therefore, a metal additive increased the surface roughness of materials, causing the contact angle to increase, which means a decrease in the hydrophilic characteristic. The contact angles in descending order were W-Ag > W-Cu > W-Co > W-Zn. This result agrees with the Ra data. Varying the metal added altered the hydrophilicity. The lowest hydrophilicity was observed for Ag, and the highest was observed for Zn.

Degree of swelling

Table 2 lists the data on the degree of the WPU swelling, depending on the metal additive. For the W-Zn result, the degree of the WPU swelling decreased from 31.2 to 30.4 %; the hydrophobicity of the various metal additives resulted in varying degrees of swelling. The decrease in the degree of swelling is caused by the WPU containing pyridyl units that generated dipolar bonds with the metal ions. The result is a metal-filled WPU with a high crystallinity, leading to a reduced hydrophilicity and degree of swelling.

Energy dispersive X-ray spectroscopy

Figure 5 reveals the EDS analysis and distribution of elements for the WPU/metal composites. Table 3 indicates the elemental wt% obtained through EDS analysis and the estimated wt% inferred from the experiment. The method of calculation is described below.

The required quantity of the metal to be added (g) = 2,6-PDM equivalent × the percentage of the metal added × the molecular weight of the metal. For the case of W-Ag, when the 2,6-PDM equivalent is 0.018, the required quantity of the Ag additive is 0.306 g (=0.018 × 10 % × 169.87).
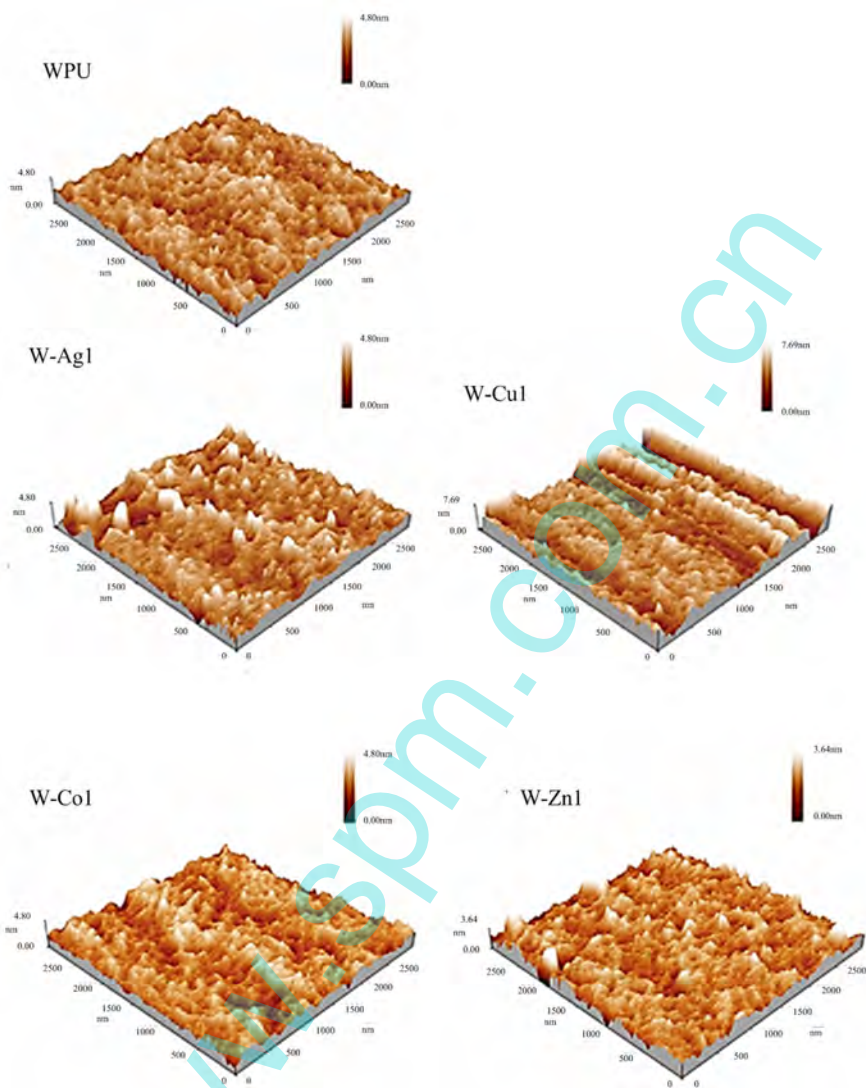
Fig. 3 AFM images of WPU films: **a** WPU, **b** W-Ag1, **c** W-Cu1, **d** W-Co1, and **e** W-Zn1

The theoretical W-Ag (wt%) = 0.306 g Ag additive/[26.03 g (0.1987, H12MDI equivalent) + 33 g (0.033, PBA equivalent) + 10.98 g (0.018, D-3403 equivalent) + 1.251 g (0.018, 2,6-PDM equivalent) + 3.698 g (0.0552, DMPA equivalent) + 2.51 g (0.0497, TEA equivalent) + 2.235 g (0.0745, EDA equivalent) + 0.306 g Ag additive] × 100 % = 0.38 %. The theoretical quantities of the metal additives (wt%) and the EDS-measured quantities (wt%) are similar (an error rate less than 2.60 %), indicating that the experimental results are comparable with the theoretical data.
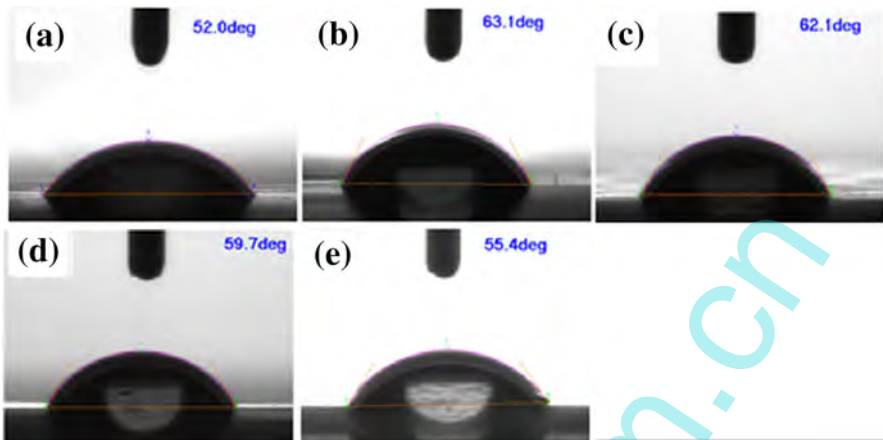
Fig. 4 Contact angles for WPU films: **a** WPU, **b** W-Ag1, **c** W-Cu1, **d** W-Co1, and **e** W-Zn1

Thermogravimetric analysis

Because of the intermolecular hydrogen bonding effect, the thermal stability of soft segments can delay the direct attacks from free radicals; the result is increased pyrolysis temperature. Petrovic et al. [32] investigated the pyrolysis phenomenon that occurred during the first interval of heating a pure WPU comprising urethane groups and urea hard segments. At least three pyrolysis peaks were produced during this interval—T_1: between 200 and 240 °C; T_2: between 240 and 300 °C; T_3: between 300 and 380 °C. Some or all of these peaks may be considered to be the pyrolysis temperatures of NCO-PBA-NCO, NCO-2,6-PDM-NCO, NCO-D3404-NCO, NCO-DMPA-NCO, and NCO-EDA-NCO. At least one pyrolysis peak (T_4: between 380 and 460 °C) and one shoulder (between 460 and 480 °C) were produced in the second interval (between 380 and 495 °C), which corresponded to the pyrolysis temperature of the soft segments (i.e., PBA, 2,6-PDM, D3404, and DMPA) [33, 34].

Figure 6a plots the TGA curves of WPUs with pyridine ring/metal composites, and the results demonstrate that the thermal stability of WPUs can be enhanced by adding metals. The initial pyrolysis temperatures for the pure WPU and WPUs containing various metals in descending order were as follows: W-Co (248.4 °C) > W-Zn (246.3 °C) > W-Cu (244.7 °C) > W-Ag (242.3 °C) > WPU (234.9 °C). These data denote that the dispersibility of the various metal ion additives affect the pyrolysis temperature of the WPUs.

Figure 6b provides the differential thermal analysis (DTA) of the various pyridine-filled WPU/metal composites, where the degraded hard segments in the first interval (between 200 and 390 °C) indicated a delayed effect (between 195 and 415 °C) with the addition of metal ions. Degraded hard segments in the second interval indicated a delay between 380–495 and 380–530 °C, and the shoulders were developed considerably. This phenomenon is due to the dispersion of the added inorganic metals in soft and hard segments, which delays the heat source
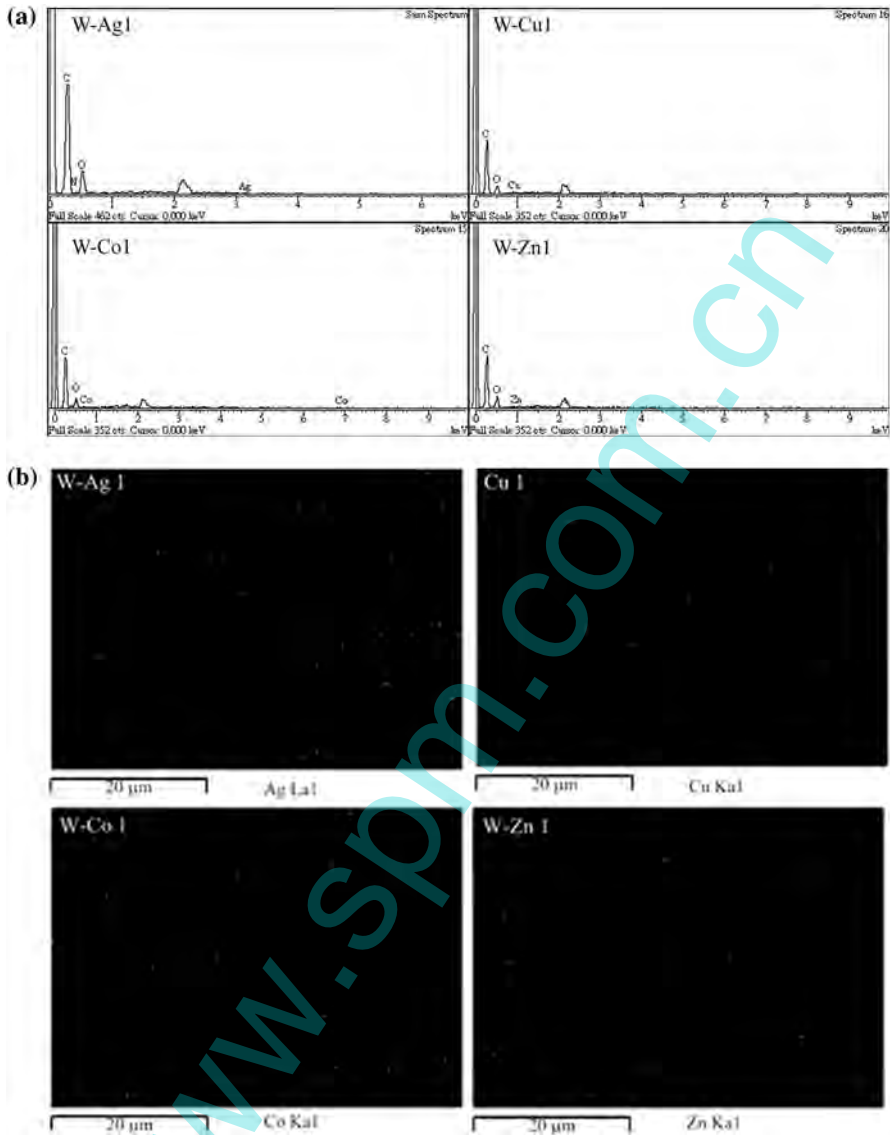
**Fig. 5 a** EDS analysis and **b** images of elemental distribution for W-Ag1, W-Cu1, W-Co 1, and W-Zn1

attacks on the hard segments. This dispersion further delays the breaking up of the urethane group bonds (i.e., the production of free radicals). When the pyrolysis of the urethane groups with hard segments is delayed, the free radical attacks on the soft segment molecules are also delayed, resulting in increased pyrolysis temperatures of both the hard and soft segments. Table 4 summarizes the collected data. The char residues of WPU/metal composites at 700 °C (Table 4) are different from the theoretical and actual weights because of the difference in the degree of

Table 3 Theoretical and experimental weights of elemental metals in WPU/metal composites

Sample	Element	Theoretical weight %[a]	Actual weight %	Error amount %[b]
W-Ag	Ag	0.38	0.37	2.63
W-Cu	Cu	0.45	0.45	0.00
W-Co	Co	0.56	0.55	1.79
W-Zn	Zn	0.49	0.48	2.04

[a] Theoretical weight % = metal/(H$_{12}$MDI + PBA + D-3403 + 2,6-PDM + DMPA + TEA + EDA + metal) × 100 %

[b] Error amount % = [(theoretical weight % − actual weight %)/theoretical weight %] × 100 %
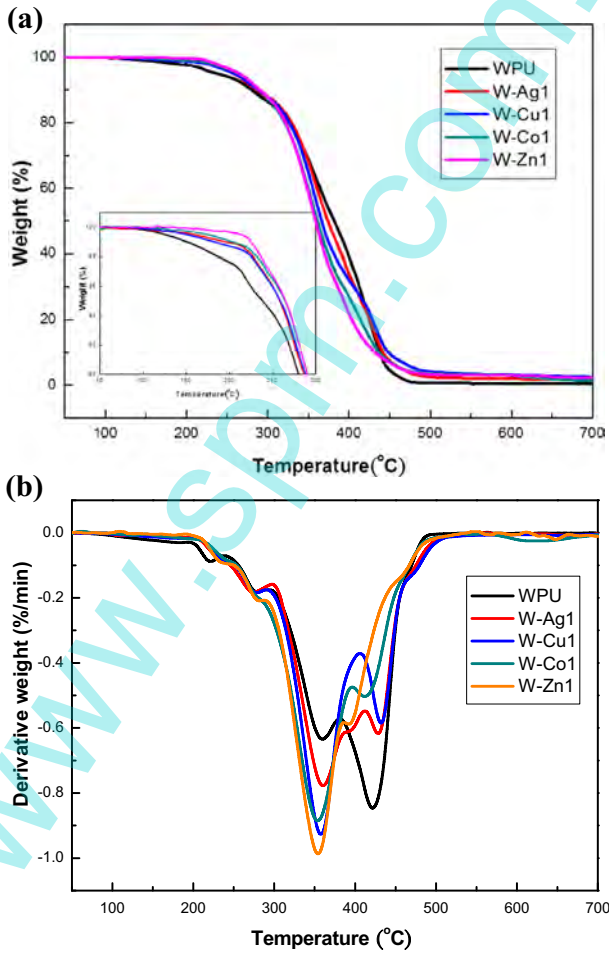
Fig. 6 a TGA and **b** DTA curves of WPU, W-Ag, W-Cu, W-Co, and W-Zn

Table 4 Pyrolysis temperatures and char residues of WPU and WPU/metal composites

Sample	TGA			DSC
	T_{onset} (°C)	T_{second} (°C)	Char residue, 700 °C (%)	T_g (°C)
WPU	234.9	334.8	0.44	−62.72
W-Ag	242.3	332.8	1.41	−57.31
W-Cu	244.7	332.6	2.56	−52.22
W-Co	248.4	332.4	1.32	−50.41
W-Zn	246.3	323.5	2.18	−50.06

T_{onset} first interval pyrolysis temperature, T_{second} second interval pyrolysis temperature

coordination of the added metals in WPUs. These data agree with those of another report [34]; the char residue for Cu was higher than that for Co in the PU at the same metal content.

Differential scanning calorimetry

DSC was used to analyze endothermic and exothermic changes (Fig. 7). WPUs were fabricated from soft and hard segments, where the T_g could be controlled using various molecular structural designs and by blending composite materials to adjust the processing temperature and applicable temperature ranges. Typical PUs from the WPUs synthesized in this experiment included the presence of soft segments with a T_g of −62.72 °C. Table 3 shows that the T_gs of the WPU soft segments increase with the addition of AgNO₃. This phenomenon can be attributed to the increased quantity of the silver nitrate, which restricts the molecular chain movement of the soft segments, leading to increased T_gs. The T_gs of the soft segments of the WPUs containing various metal ions in descending order were as follows: W-Zn (−50.06 °C) > W-Co (−50.41 °C) > W-Cu (−52.22 °C) > W-Ag (−57.31 °C) > WPU (−62.72 °C). These results mean that the T_gs of the soft segments can be elevated by adding metals.

Dynamic mechanical analysis

DMA results pertain to the loss modulus E'' (Fig. 8), storage modulus E' (Fig. 9), and tan δ (Fig. 10) of the WPU/metal composites. The E' of WPUs at −70 °C was 3195.4 MPa, which falls under the category of being glassy, a characteristic of hard and brittle materials. When the temperature increased to −53.75 °C, a reduction of 1–2 orders of magnitude was experienced. The first transition zone (−48.52 °C) in the E'' graph can be understood as the glass transition temperature of the soft segment region (T_g-S), where the peak value of tan δ was −43.05 °C. By increasing the temperature of the T_g-S transition zone, the value of E' gradually declined and was reduced to 99.6 MPa at 25 °C. The category is rubber-like, a characteristic shared by soft materials. Using a macroscopic observation, the material was shown to be solid, and closer microscopic inspections revealed that the soft segments possessed rubber-like stickiness and liquid-like flow. In addition, the hard segments
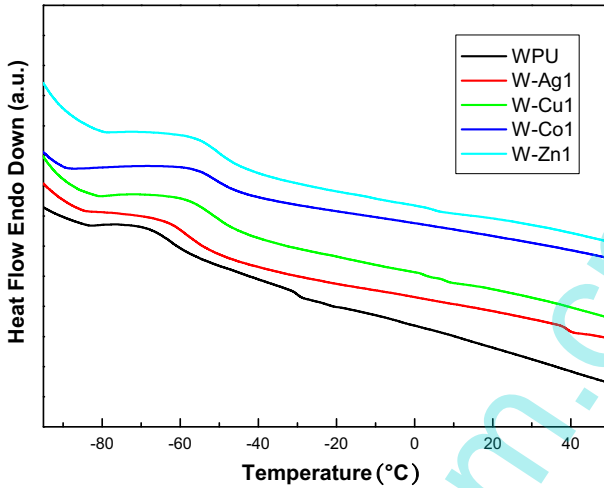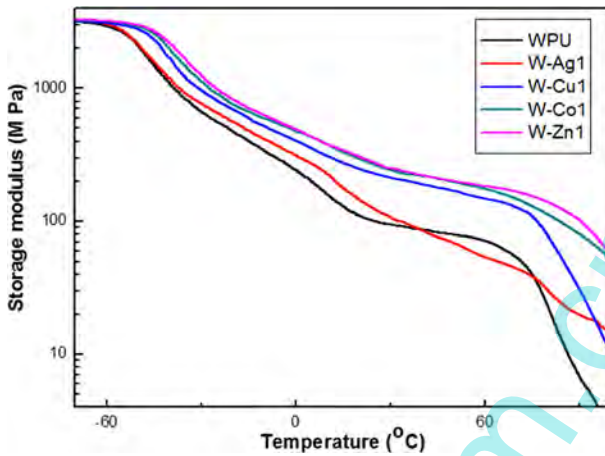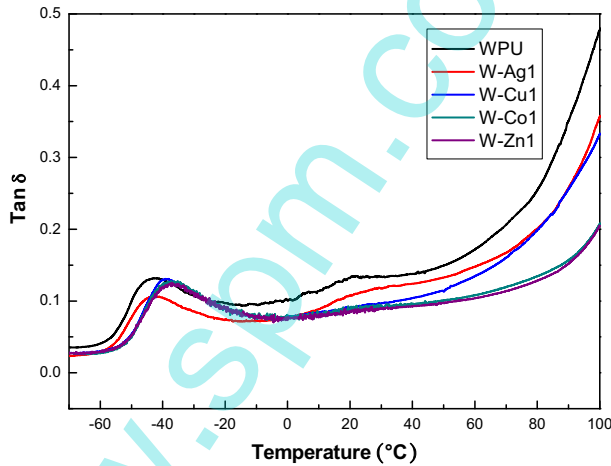
Fig. 7 DSC of WPU and WPU/metal composites
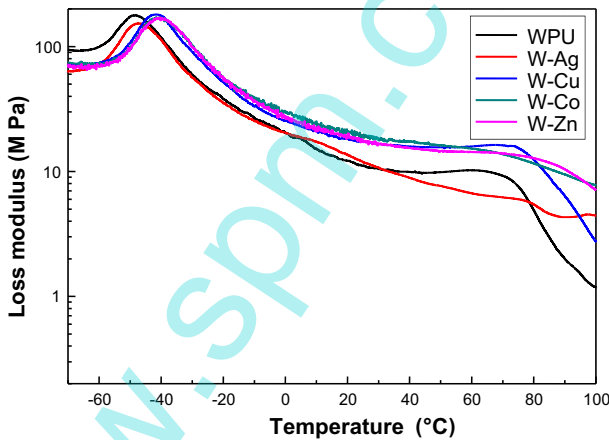
Fig. 8 Loss modulus for WPU and WPU/metal composites

remained glassy. This behavior signified that the WPUs possessed structural characteristics of a micro-phase separation. When the temperature was increased to 61.08 °C, the E' underwent further reduction, which was observed through the E''. A shoulder appeared when the onset point was 69.17 °C. This high-temperature transition zone can be viewed as an α' transfer, which signifies the glass transition zone of the hard segments (T_g-H) [35]. As shown in Table 5, the E' value of W-Ag increased from 3195.4 to 3436.9 MPa at −70 °C and from 99.6 to 162.1 MPa at 25 °C (room temperature), indicating that adding a metal can enhance the material rigidity. When the temperature reached the T_g-S transition zone, the E' of W-Ag dropped to a temperature of −52.77 °C (tan δ = −42.18 °C); the E' of W-Cu was reduced to a temperature of −48.66 °C (tan δ = −38.94 °C); the E' of W-Co was

Fig. 9 Storage modulus for WPU and WPU/metal composites

Fig. 10 Tan δ graph for WPU and WPU/metal composites

reduced to a temperature of -46.32 °C (tan $\delta = -37.30$ °C); and the E' of W-Zn dropped to a temperature of -45.76 °C (tan $\delta = -36.69$ °C). These results are caused by the dipolar bonds created by the metals and pyridine rings, which restrict the molecular chain activities, resulting in increase in the T_g-S. In the T_g-H transition zone, the E'' shoulder moved to higher temperature regions (e.g., W-Ag: 78.37 °C; W-Cu: 74.35 °C; W-Co: 72.65 °C; and W-Zn: 81.96 °C) because of the ion interactions that occurred between the metal ions and the ions from the hard segment regions of the WPUs. This behavior resulted in a slight increase in the T_g-H. Table 5 shows the T_g-S (E'') results in descending order: W-Zn (-45.76 °C) > W-Co (-46.32 °C) > W-Cu (-48.66 °C) > W-Ag (-52.77 °C) > WPU (-53.75 °C), which match the T_g order in the DSC described in the

Table 5 Data on glass transition temperatures (as measured by DMA) of WPU and WPU composites containing different metals and on storage modulus at low (<0 °C) and high (room) temperatures

| Sample	Glass transition temperature (°)			Storage modulus (MPa)	
	T_g-S		T_g-H	−70 °C	25 °C
	Storage modulus	Tan δ	Loss modulus		
WPU	−53.75	−43.05	69.17	3195.4	99.6
W-Ag	−52.77	−42.18	78.37	3436.9	162.1
W-Cu	−48.66	−38.94	74.35	3217.5	230.9
W-Co	−46.32	−37.30	72.65	3253.9	266.7
W-Zn	−45.76	−36.69	81.96	3263.1	274.4

previous section. The T_g-H (E'') results in descending order were W-Zn (81.96 °C) > W-Ag (78.37 °C) > W-Cu (74.35 °C) > W-Co (72.65 °C) > WPU (69.17 °C).

Tensile properties

Figure 11 plots the stress-strain graph of various WPU samples obtained using an extension test. The maximum break stress, Young's modulus, and strain at break of WPUs were 15, 86 MPa, and 800 %, respectively. These results illustrate the soft and flexible material characteristics. By adding metal ions, both Young's modulus and break stress increased, but the strain at break decreased. These results are caused by the following: the dipolar bonds created by the WPU pyridine rings and metals enhanced the intermolecular forces between the molecules and enabled the materials to withstand higher stresses without deforming. This behavior makes the materials stronger. The maximum break stresses for the various specimens in descending order were W-Ag > W-Zn > W-Co > W-Cu > WPU. Table 6 provides the average data obtained from the experiment. By adding various metals, the mechanical strength of WPUs was enhanced. However, this addition caused the material flexibility and ductility to decrease.

Antimicrobial properties

Table 7 shows the inhibition zones for the pyridine-filled WPU/metal composite films toward *S. aureus* and *K. pneumoniae*. The table indicates that the WPU containing silver nitrate possessed antibacterial properties against *S. aureus*. The reason why copper acetate and zinc acetate do not show antibacterial properties is the low quantity of the additives used, resulting in a low concentration of the metal ions and the inability to effectively suppress bacteria. Ag^+, however, is effective when its ions are slowly and gradually released, and it is capable of destroying bacterial cell membranes even at very low concentrations. In addition, it can attract and rapidly bond with the sulfhydryl group of the bacterial enzyme proteins, suppressing the synthesis of bacterial proteins and nucleic acids. The result is
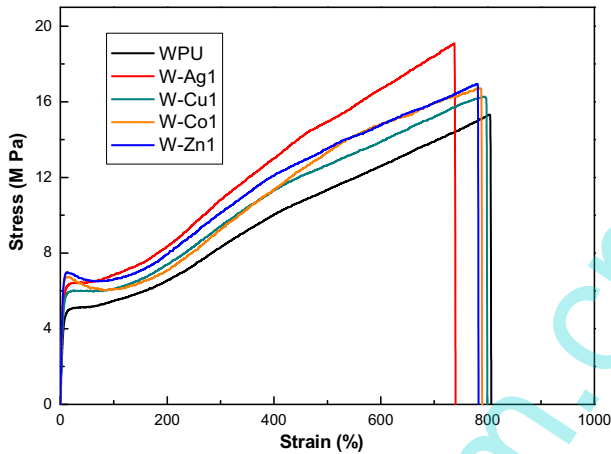
Fig. 11 S–S curves of WPU and WPU/metal composites

Table 6 Tensile strength, Young's modulus, and elongation at break of WPU and WPU composites with various metals

Sample	Break stress (MPa)	Young's modulus (MPa)	Strain at break (%)
WPU	15.3	86.4	803.6
W-Ag	19.1	108.3	738.1
W-Cu	16.3	106.7	797.5
W-Co	16.8	121.6	788.9
W-Zn	17.0	137.2	781.3

Table 7 Antibacterial effects of WPU and WPU composites with various metals

Sample	Zone of inhibition (mm)	
	S. aureus	*K. pneumoniae*
WPU	0	0
W-Ag	1.2	0
W-Cu	0	0
W-Co	0	0
W-Zn	0	0

lowered activity of the active enzymes within the protozoa, which prolongs the antibacterial effect [1, 29].

Water vapor permeability and waterproofness analyses of fabrics coated with waterborne polyurethane

Table 8 presents the data on the waterproofness and WVP of various nylon fabric samples with and without WPU coating. The results demonstrate that the WVP for the

Table 8 Waterproofness and water vapor permeability of WPU and WPU/metal composites

Sample	Waterproofness (mm H_2O)	WVP (g/m^2 × 24 h)
F	–	10,000
F-WPU	1200	4328
F-W-Ag	2075	3140
F-W-Cu	2020	3310
F-W-Co	1830	3564
F-W-Zn	1535	3649

coated fabrics was less than that for the non-coated fabrics and that it was reduced with the addition of metals. It is concluded that this study successfully produced WPU coatings possessing characteristics of waterproofness and WVP. Furthermore, it is discovered that coating the fabrics with the WPU emulsion containing high-level metals enhances the waterproofness and reduces the WVP. The waterproofness of the WPU composites produced from various metals in descending order was W-Ag > W-Cu > W-Co > W-Zn. This result indicates that various metals possess differing effects on the waterproofness of the WPUs coated on the fabrics, with Ag possessing the highest waterproofness and Zn the lowest waterproofness.

Conclusions

This study adopted a molecular structure design concept, and on the basis of the synthetic organic chemistry and high polymer synthesis method, composite materials were formed by inserting pyridine molecule groups in the WPU and by adding inorganic metals. This study applied different metal ions (W-Zn, W-Co, W-Cu, and W-Ag) to fabricate WPUs and to investigate the effects of these metals on the WPU properties. Using a Fourier transform infrared spectrometer to identify their structure, it was observed that compounds possessed high water solubility and low viscosity, indicating good aqueous solution processability. The particle size and viscosity analyses revealed that the WPU particle size increased from 113 to 219 nm and the viscosity increased from 9.5 to 11.6 cps with the addition of various metals. These results mean that adding metals reduces the aqueous solution processability. The EDS analysis showed that the actual quantities of the elemental metals were similar to the theoretical quantities. AFM demonstrated that adding metals changed the material surface features and increased the roughness, and these changes further affected the material surface contact angles. The contact angle and degree of swelling tests indicated that the various metals increased the WPU contact angles from 52.0° to 63.1°, whereas the degree of swelling was reduced from 31.2 to 29.8 %. These changes enhanced the material hydrophobicity. The TGA test results illustrated that the WPU pyrolysis temperature increased when various metals were added and that the WPU with Co possessed the best thermal stability. The DSC and DMA analyses indicated that small amounts of metals could slightly increase the T_g-S and T_g-H. An extension test showed that the metals enhanced the mechanical strength of WPUs and increased the Young's modulus from 86 to 137 MPa. In addition, the WPU with Ag possessed

the strongest mechanical strength. For antibacterial tests, the results denoted that the WPU groups containing silver nitrate possessed strong antibacterial properties. The water vapor permeability and waterproofness analyses showed that the WPU/metal composites possessed characteristics of waterproofness and WVP. Consequently, the WPUs with pyridine rings generated dipolar bonds with the metal ions (Ag, Cu, Co, and Zn), and adding a metal to a WPU containing pyridine rings enhanced the WPU thermal stability, mechanical strength, and hydrophobicity. The characteristics of Co and Ag were as follows: Co provided the best thermal stability; Ag provided the best mechanical strength and imparted antibacterial properties. Regarding the fabric coating, the WPU containing the silver metal possessed the best waterproofness with less WVP, and the WPU containing the cobalt metal possessed the highest WVP with less waterproofness.

References

1. Kim BK (1996) Aqueous Polyurethane Dispersions. Colloid Polym Sci 275(4):599–611
2. Chen GN, Chen KN (1997) Self-Curing Behaviors of Single Pack Aqueous-Based Polyurethane System. J Appl Polym Sci 63(12):1609–1623
3. Diterich D, Keberie W, Witt H (1970) Polyurethane Ionomers, a New Class of Block Polymers. Chem Int Ed Engl 9(1):40–50
4. Coutinho FMB, Delpech MC (1996) Some Properties of Films Cast from Polyurethane Aqueous Dispersions of Polyether-Based Anionomer Extended with Hydrazine. Polym Testing 15(2):103–113
5. Delpech MC, Coutinho FMB (2000) Waterborne anionic polyurethanes and poly(urethane-urea)s: influence of the chain extender on mechanical and adhesive properties. Polym Testing 19(8):939–952
6. Shao CH, Huang JJ, Chen GN, Yeh JT, Chen KN (1999) Thermal and combustion behaviors of aqueous-based polyurethane system with phosphorus and nitrogen containing curing agent. Polym Degrad Stab 65(3):359–371
7. Datta J, Pasternak S (2005) Oligourethane glycols obtained in glycolysis of polyurethane foam as semi-finished products for cast urethane elastomers preparation. Polimery 50(5):352–357
8. Datta J, Glowinska E (2014) Chemical modifications of natural oils and examples of their usage for polyurethane synthesis. Journal of Elastomers and Plastics 46(1):33–42
9. Datta J, Glowinska E (2014) Effect of hydroxylated soybean oil and bio-based propanediol on the structure and thermal properties of synthesized bio-polyurethanes. Ind Crops Prod 61:84–91
10. Tsou CH, Lee HT, De Guzman M, Tsai HA, Wang PN, Cheng HJ, Suen MC (2015) Synthesis of biodegradable polycaprolactone/polyurethane by curing with H_2O. Polym Bull 72:1545–1561
11. Tsou C-H, Suen M-C, Yao W-H, Yeh J-T, Wu C-S, Tsou C-Y, Chiu S-H, Chen J-C, Wang RY, Lin S-M, Hung W-S, De Guzman M, Hu C-C, Lee K-R (2014) Preparation and characterization of bioplastic-based green renewable composites from tapioca with acetyl tributyl citrate as a plasticizer. Materials. 7(8):5617–5632
12. Mohamed HA, Badrana BM, Rabieb AM, Morsi SMM (2014) Synthesis and characterization of aqueous (polyurethane/aromatic polyamide sulfone) copolymer dispersions from castor oil. Prog Org Coat 77(6):965–974
13. Hsu SH, Tang CM, Tseng HJ (2006) Biocompatibility of poly(ether)urethane-gold nanocomposites. J Biomed Mater Res A 79A(4):759–770
14. Grady BP (2010) Recent developments concerning the dispersion of carbon nanotubes in polymers. Macromol Rapid Commun 31(3):247–257

15. Hunley MT, Potschke P, Long TE (2009) Melt dispersion and electrospinning of nonfunctionalized multiwalled carbon nanotubes in thermoplastic polyurethane. Macromol Rapid Commun 30(24):2102–2106
16. Jana RN, Cho JW (2008) Thermal stability and molecular interaction of polyurethane nanocomposites prepared by in situ polymerization with functionalized multiwalled carbon nanotubes. J Appl Polym Sci 108(5):2857–2864
17. Mu C, Zhang L, Song Y, Chen X, Liu M, Wang F, Hu X (2016) Modification of carbon nanotubes by a novel biomimetic approach towards the enhancement of the mechanical properties of polyurethane. Polymer 92:231–238
18. Hsu S, Tseng H-J, Lin Y-C (2010) The biocompatibility and antibacterial properties of waterborne, polyurethane-silver nanocomposites. Biomaterials 31:6796–6808
19. Kuan HC, Ma CCM, Chang WP, Yuen SM, Wu HH, Lee TM (2005) Synthesis, thermal, mechanical and rheological properties of multiwall carbon nanotube/waterborne polyurethane nanocomposite. Compos Sci Technol 65:1703e10
20. Hsu SH, Chou CW, Tseng SM (2004) Enhanced thermal and mechanical properties in polyurethane/ Au nanocomposites. Macromol Mater Eng 289(12):1096–1101
21. Zhao C-X, Zhang W-D, Mai A-P, Huang X-M, Ouyang YS (2011) Synthesis and characterization of waterborne polyurethane/Cu(II)-loaded hydroxyapatite nanocomposites with antibacterial activity. J Nanosci Nanotechnol 11(8):6779–6787
22. Ma Xue-Yong, Zhang Wei-De (2009) Effects of flower-like ZnO nanowhiskers on the mechanical, thermal and antibacterial properties of waterborne polyurethane. Polym Degrad Stab 94:1103–1109
23. Cao XD, Dong H, Li CM (2007) New nanocomposite materials reinforced with flax cellulose nanocrystals in waterborne polyurethane. Biomacromolecules 8(3):899–904
24. Wu QJ, Henriksson M, Liu X, Berglund LA (2007) A high strength nanocomposite based on microcrystalline cellulose and polyurethane. Biomacromolecules 8(12):3687–3692
25. Bayer IS, Steele A, Martorana PJ, Loth E (2010) Fabrication of superhydrophobic polyurethane/ organoclay nano-structured composites from cyclomethicone-in-water emulsions. Appl Surf Sci 257(3):823–826
26. Choi HY, Bae CY, Kim BK (2010) Nanoclay reinforced UV curable waterborne polyurethane hybrids. Prog Org Coat 68(4):356–362
27. Lee HT, Lin LH (2006) Waterborne polyurethane/clay nanocomposites: novel effects of the clay and its interlayer ions on the morphology and physical and electrical properties. Macromolecules 39(18):6133–6141
28. Datta J, Laski M, Kucinska-Lipka J (2007) The properties of polyurethane elastomers to be used as polymer cores in sandwich plate systems (SPS). Przem Chem 86(1):63–67
29. Meng QB, Lee S-I, Nah C, Lee Y-S (2009) Preparation of waterborne polyurethanes using an amphiphilic diol for breathable waterproof textile coatings. Prog Org Coat 66:382–386
30. Tsou CH, Lee HT, Hung WS, Wang CC, Shu CC, Suen MC, De Guzman M (2016) Synthesis and properties of antibacterial polyurethane with novel bis(3-pyridinemethanol) silver chain extender. Polymer 85:96–105. doi:10.1016/j.polymer.2016.01.042
31. Tsou CH, Lee HT, Tsai HA, Cheng HJ, Suen MC (2013) Synthesis and properties of biodegradable polycaprolactone/polyurethanes by using 2,6-pyridinedimethanol as a chain extender. Polym Degrad Stab 98:643–650
32. Petrovic ZS, Zavargo Z, Flynn JH, Macknight WJ (1994) Thermal degradation of segmented polyurethanes. J Appl Polym Sci 51:1087–1095
33. Shubiao Z, Huiming J, Yingmei X, Donghui Z (2007) Thermal and crystalline properties of waterborne polyurethanes based on IPDI, DMPA, and PEBA/HNA. J Appl Polym Sci 103:1936–1941
34. Lee H-T, Wu S-Y, Jeng R-J (2006) Effects of sulfonated polyol on the properties of the resultant aqueous polyurethane dispersions. Colloids Surf A: Physicochem Eng Asp 276:176–185
35. Senthilkumar N, Raghavan A, Sultan Nasar A (2005) Novel metal-containing polyurethane elastomers prepared using tetradentate schiff base metal complexes. Macromol Chem Phys 206:2490–2500